Laser ablation of $(GeSe_2)_{100-x}(Sb_2Se_3)_x$ chalcogenide glasses: Influence of the target composition on the plasma plume dynamics

S. Irimiciuc[1,2], R. Boidin[3], G. Bulai[2,4*] georgiana.bulai@uaic.ro, S. Gurlui[2], P. Nemec[3], V. Nazabal[5], C. Focsa[1]

[1]Laboratoire de Physique des Lasers, Atomes et Molécules (UMR CNRS 8523), Université de Lille 1 Sciences & Technologies, 59655 Villeneuve d'Ascq, France

[2]Faculty of Physics, LOA-SL, "Al. I. Cuza" University of Iasi, Romania

[3]Faculty of Chemical Technology, University of Pardubice, Studentska 573, 53210 Pardubice, Czech Republic

[4]Integrated Centre for Environmental Science Studies in the North-East Development Region - CERNESIM, "Al. I. Cuza" University of Iasi, Romania

[5]Institut des Sciences Chimiques de Rennes (UMR CNRS 6226), Université de Rennes 1, 35042 Rennes, France

*Corresponding author.

Highlights

- ICCD images revealed the presence of three structures with distinct dynamics
- Space and time resolved OES measurements revealed the nature of each structure
- Increased velocities of all three structures were observed for Sb rich samples
- Excitation temperatures obtained by Boltzmann plots increased as Sb_2Se_3 was added
- Plasma characteristics were correlated to the properties of the bulk samples

The dynamics and properties of the $(GeSe_2)_{100-x}(Sb_2Se_3)_x$ laser-induced plasma were investigated by fast ICCD imaging and space- and time-resolved optical emission spectroscopy (OES). The experiments were performed at 10^{-6} Torr background pressure, using the second harmonic (532 nm) of the Nd-YAG laser (10 ns, 10 Hz). For all investigated samples, the ICCD images revealed a splitting of the plasma plume into three components with distinct dynamics. Based on OES measurements, the first and second plasma structures were found to be represented mainly by ionic and neutral species, respectively. As the Sb_2Se_3 content of the samples increases, the three structures present an increase in their velocities. This dynamic variation and also the compositional dependence of the excitation temperature obtained from Boltzmann plots were correlated to the changes in the structure and electrical/thermal properties of the bulk chalcogenide glasses.

1. INTRODUCTION

Amorphous chalcogenides present unique optical properties (low phonon energies, high optical transparency in IR region, high linear and nonlinear refractive index, photosensitivity) making them very interesting for different applications in the civil, medical or military areas [1-3]. Chalcogenide glasses and thin films are known to be particularly sensitive to light irradiation; commonly observed photoinduced phenomena involve changes in optical properties (band gap energy changes [4,5] or refractive index modifications [6]), however other photoinduced phenomena such as photodiffusion [7], photofluidity [8] and photocrystallization [9] were reported as well. Photosensitivity of amorphous chalcogenides is caused by their structural flexibility and electronic lone-pair p states forming the top part of their valence band [2, 10]. All mentioned effects are observed in bulk materials; however they are particularly pronounced in thin films. One of the reasons is that film can condense into amorphous state with a large number of defective bonds, creating a different topology from that of bulk glasses [11].

For some applications like plasmon/soliton waveguides, it is necessary to design amorphous chalcogenide layers which possess high nonlinear refractive index (n_2) and low two photon absorption coefficient (β). For high optical nonlinearities, As-S(Se,Te) and Ge-(As)-S(Se,Te) glass systems were mainly studied [12-16]. However, due to presence of arsenic, which is toxic in its elemental form, arsenic-containing compositions are environmentally unacceptable [17]. That is why germanium is considered as other suitable glass network former. Based on the applications-driven requirements, such as excellent transparency in mid-IR (especially in 8-12 μm window), large (non)linear refractive index, and good glass-forming ability, the choice of Ge-Se system seems to be favorable in comparison with Ge-S or Ge-Te ones. Following literature data, selenium-based glasses generally seem to be a good compromise because they have larger n_2 than sulfur based glasses [15] and less important β than tellurium based glasses [18]. The glass-forming ability and physical properties of Ge-Se glasses can be further enhanced and tailored by their alloying with antimony. Partial substitution of Ge with Sb may result in an increase of the (non)linear refractive index of the corresponding amorphous chalcogenides due to the enlargement of (hyper)polarisability. This hypothesis was confirmed in our previous work, where we described the nonlinear properties of $(GeSe_2)_{100-x}(Sb_2Se_3)_x$ bulk glasses at 1.064 μm as well as at 1.55 μm, concluding that the addition of Sb_2Se_3 to $GeSe_2$ leads to the increase of n_2 and β [19].

However, the development of integrated optical devices for nonlinear applications based on chalcogenide materials requires amorphous chalcogenides in thin film form. Different deposition techniques such as thermal evaporation [17], radio-frequency (rf) magnetron sputtering [20, 21] or pulsed laser deposition (PLD) [20] are available for the fabrication of amorphous Ge-Sb-Se thin films. PLD method is considered as one of the prospective techniques in the field according to its simplicity, easy control of the process and often stoichiometric transfer of the material from the target to the film [22, 23]. Although the PLD technique for chalcogenide thin films' growth has been employed for more than two decades [5], the optimization of the deposition parameters is generally made in an empirical manner. This is probably connected with the fact that the optimization of the PLD parameters requires a detailed understanding of the processes proceeding in the plasma (formed due to the interaction of the laser pulse with the chalcogenide material) during the deposition, which is usually missing. The characterization of the plasma plume being formed during laser ablation is thus highly desirable.

The aim of this work was to investigate the behavior of plasma plume generated by nanosecond laser ablation of $(GeSe_2)_{100-x}(Sb_2Se_3)_x$ (where x varies from 0 to 60%) chalcogenide glasses under vacuum. The formation and dynamics of the laser induced plasma were investigated through fast gate ICCD imaging and time- and space-resolved optical emission spectroscopy (OES). From the space-time evolution of the optical signals, the velocities of various species present in the plasma (including neutrals and ions) were derived. The obtained results were correlated to the Sb content in the bulk materials. The gained knowledge should contribute to a better understanding of the fabrication and properties of thin $(GeSe_2)_{100-x}(Sb_2Se_3)_x$ amorphous films prepared by PLD.

2. EXPERIMENTAL DETAILS

Bulk samples from pseudo-binary $(GeSe_2)_{100-x}(Sb_2Se_3)_x$ system (where x varies from 0 to 60%) were synthesized by conventional melting and quenching technique using high purity (5N) elements Ge, Sb, and Se [19]. Individual chemical composition and atomic ratios are listed in Table 1. The obtained glass rods were annealed at 200°C below their glass transition temperature (T_g) for 6 hours and then slowly cooled down to room temperature. For our experiments the resulting glass rods (25 mm in diameter) were sliced and polished.

TABLE I. Chemical compositions of the used chalcogenide $(GeSe_2)_{100-x}(Sb_2Se_3)_x$ targets.

Sb_2Se_3 concentration (x %)	Composition	Ge:Sb:Se ratio
0	$Ge_{33.3}Se_{66.7}$	1:0:2
10	$Ge_{28.1}Sb_{6.3}Se_{65.6}$	1:0.22:2.33
20	$Ge_{23.5}Sb_{11.8}Se_{64.7}$	1:0.5:2.8
30	$Ge_{19.4}Sb_{16.7}Se_{63.9}$	1:0.86:3.3
40	$Ge_{15.8}Sb_{21.1}Se_{63.2}$	1:1.33:4
50	$Ge_{12.5}Sb_{25}Se_{62.5}$	1:2:5
60	$Ge_{9.5}Sb_{28.6}Se_{61.9}$	1:3:6.5

In order to study the laser ablation process on the chalcogenide glasses the experimental set-up shown in Figure 1 was employed [24, 25]. The experiments were performed in a stainless steel vacuum chamber at a residual pressure of 10^{-6} Torr. The second harmonic from a Nd:YAG laser (532 nm, 10 ns, 10 Hz) was focused on the chalcogenide target at normal incidence by a f = 25 cm lens placed outside the vacuum chamber. The estimated diameter of the impact area was 1 mm and the laser energy was set at 20 mJ/pulse, leading to a laser fluence of ~2.7 J/cm^2. A metallic substrate was placed at a distance of 4.3 cm in front of the target. The fluence and the target-substrate distance were chosen as to study the plasma dynamics under conditions close to PLD configuration used previously for $(GeSe_2)_{100-x}(Sb_2Se_3)_x$ (x=0-60%) thin film deposition [26]. Both the target and the substrate were electrically isolated. A 5 mm x 10 mm slit was made in the substrate center to ensure a normal incidence irradiation. The target, substrate and laser focusing lens were attached to the same XYZ micrometric translation stage, thus allowing the translation of the whole system for space-resolved measurements. This arrangement also ensures the same ablation spot diameter on the target (the same fluence) for all performed experiments.

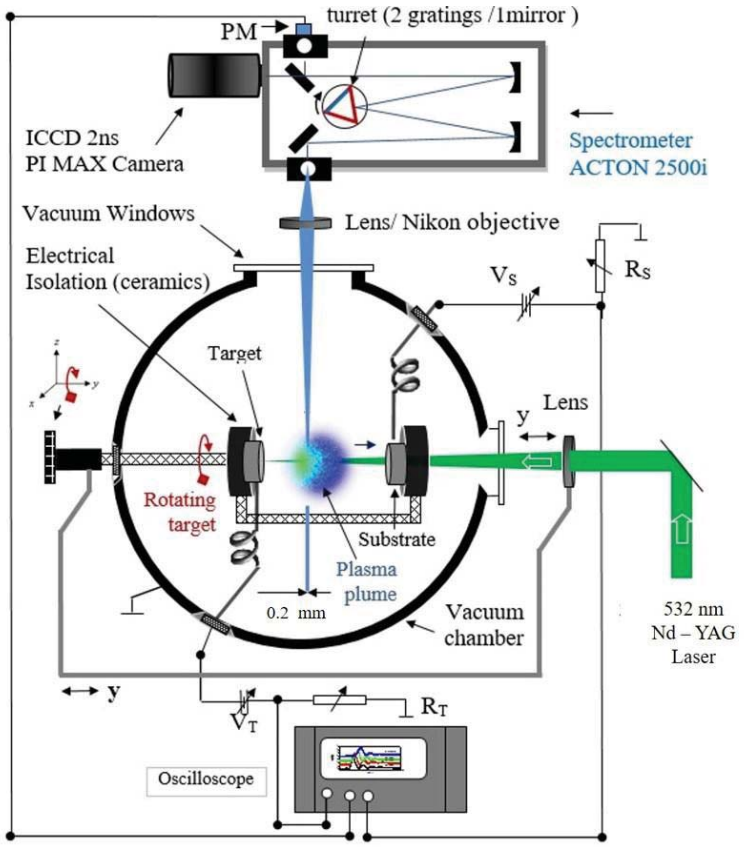

FIG. 1. Schematic view of the experimental set-up

For optical and spectral diagnostics on the laser-induced plasma, we used a Princeton Instruments ICCD camera (PIMAX2-1003-UNIGEN2, 1024 × 1024 pixels, minimum gate width 2 ns) and a Hamamatsu photomultiplier Model PD-439 (3 ns response time, working in the 185-900 nm spectral range), both coupled with a high-resolution monochromator (Acton SP2558). The monochromator is fitted with one mirror and two diffraction gratings (300 l/mm, blaze at 300 nm, and 2400 l/mm, blaze at 240 nm) mounted on the same three-position turret, which allows an easy switching between imaging mode, low-resolution and high-resolution spectroscopy experiments. The slits placed at the entrance and side exit of the monochromator can be adjusted to define the bandpass or spectral resolution required.

The global emission of the induced plasma was investigated with the turret fixed in mirror position. The ICCD images were recorded using a Nikon objective placed at the entrance of the monochromator while the slit was removed. The ICCD camera was triggered by a fast response photodiode placed outside the vacuum chamber, and an internal routine was used to increment the delay between the laser pulse and the ICCD gate opening. The images were acquired using a gate width of 20 ns, ensuring a good signal to noise ratio.

The global emission spectra were collected in the high-resolution regime at a distance of 6 mm from the target and at 25 ns gate delay. The Nikon objective was replaced with a 10

cm focusing lens and the monochromator entrance slit was set at 0.04 mm. The plasma plume was imaged by the lens on the entrance slit with a magnification of 0.2x. Considering the entrance slit width of 0.04 mm, this leads to a spatial resolution in the plasma plume of 0.2 mm. To obtain a good contrast between the emission line intensities and the background noise level presented in the collected spectra, a 2 μs gate width was used. The spatial and temporal profiles of the investigated emission lines were studied using the PM mounted at the side exit of the monochromator (with 2400 l/mm diffraction grating) and its entrance slit width was set at 0.17 mm (ensuring a 0.3 nm spectral resolution).

3. EXPERIMENTAL RESULTS

3.1. ICCD imaging

The global dynamics of the plasma originating from the interaction of the laser pulse with Ge-Sb-Se glasses was studied by recording ICCD images (20 ns gate width) at different delays after the laser pulse. As an example, sequential snapshots of the expanding $GeSe_2$ and $(GeSe_2)_{40}(Sb_2Se_3)_{60}$ plume are presented in Figure 2. The ICCD images recorded for all samples revealed a splitting process of the plasma plume into three components. The splitting process was previously evidenced in laser induced plasma of other chalcogenide systems [24, 27], however only two structures were observed. In our study, a third plume component, close to the target, with well-defined interface and large contact area with the surface was found. This behavior was also reported by Canulescu et al. when studying laser ablation of $LiMn_2O_4$ in low vacuum [28]; it was associated to multiple scattering interactions which determine a decrease of the velocity of the ejected particles. The study of Amoruso et al. [29] also revealed a third plasma structure with a wide velocity distribution below 10^2 m/s. They considered this structure to be formed by nanoparticles and characterized by a blackbody-like emission.

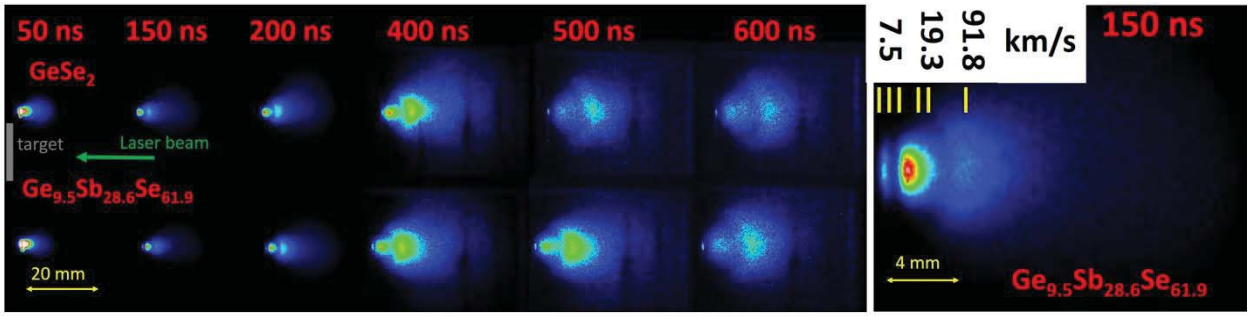

FIG. 2. ICCD images of laser produced plasmas on $GeSe_2$ and $Ge_{9.5}Sb_{28.6}Se_{61.9}$ using a gate width of 20 ns

For more information on the plume expansion dynamics and its evolution with the Sb_2Se_3 concentration, the velocities of the three plasma components were calculated by measuring the displacement of the maximum emission point at different delays. Figure 3(a-c) presents the dependence of the calculated expansion velocities with Sb_2Se_3 concentration and Ge:Sb ratio.

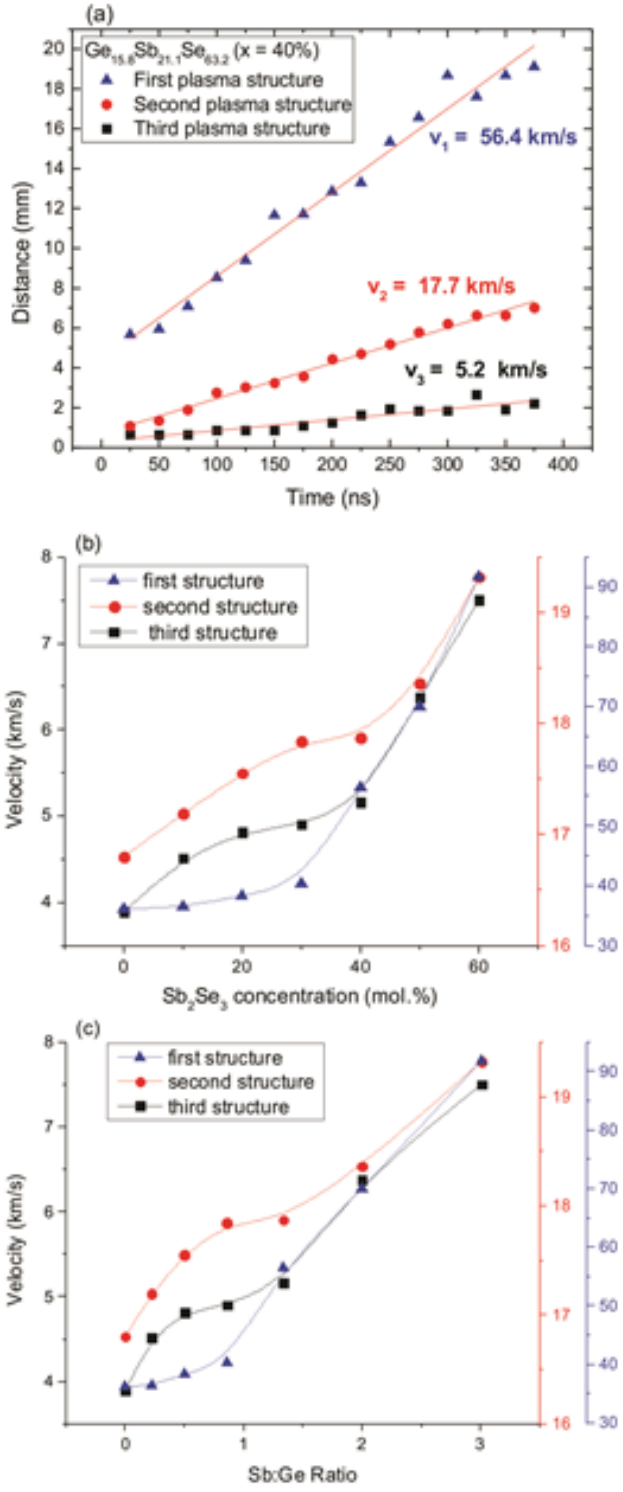

FIG. 3. The maximum emission point displacement in time (a) and the dependence between the expansion velocity on (b) Sb_2Se_3 concentration and (c) Sb:Ge ratio

The velocities of all three plasma components increase with the Sb_2Se_3 content reaching at x=60% maximum values of 92, 19 and 8 km/s for the first, second and third

components, respectively. Considering that the experiments were done under identical experimental conditions (pressure and laser fluence), the evolution of the expansion velocities would be correlated to the changes in structural and electrical/thermal properties of the bulk samples, which will be discussed in the next section.

Considering the complex structure and dynamics of the laser-produced plasma within studied chalcogenide glasses, complementary space- and time-resolved optical diagnostics of the individual plasma plume components were performed.

3.2. Space- and time-resolved optical emission spectroscopy

To analyze the contributions of different species found in the plasma plume, a spatio-temporal resolved spectroscopic study was performed. First, global emission spectra of a 0.2 mm wide plasma slice situated at 6 mm from the target surface was recorded in the 300-700 nm spectral region. Figure 4 presents an example of the emission spectra recorded for the $(GeSe_2)_{40}(Sb_2Se_3)_{60}$ target. All the observed emission lines were identified using the available database [30] as corresponding to both excited and ionized states of the three elements.

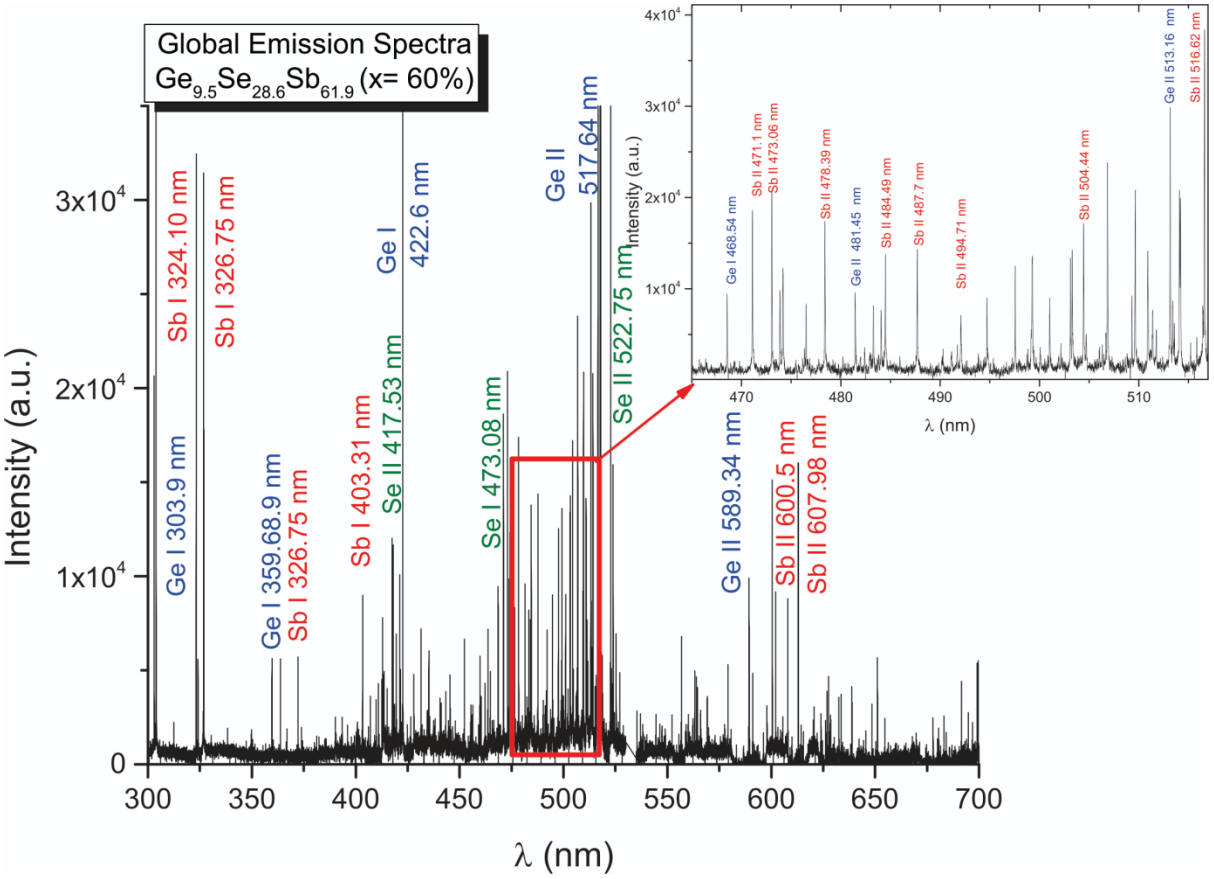

FIG. 4. Typical emission spectrum of the $(GeSe_2)_{40}(Sb_2Se_3)_{60}$ laser ablation plasma at 6 mm from the target (25 ns gate delay, 2 µs gate width)

Assuming that the emission intensity is proportional to the density of the corresponding element in the plume [31], qualitative information on the influence of the Sb_2Se_3 addition on the plasma structure can be obtained by investigating the changes in spectral line intensities (Figure 5). We observed a decrease in Ge emission line intensity (Ge I-303.9 nm: E_k 4.96 eV– E_i 0.88 eV and Ge II-517.86 nm: E_k 12.43 eV – E_i 10.08 eV) and an increase in those of Sb (Sb I 326.75nm: E_k 5.82 eV– E_i 2.03 eV and Sb II 600.5 nm: E_k 10.68 eV – E_i 8.62 eV) with the increase of the Sb_2Se_3 content. The variations recorded for Se (Se I 473.08nm and Se II 522.75 nm) were smaller than the ones found for the other two elements. These dependences are in line with the compositional changes of the bulk materials (Table 1) where only a 4.8% decrease in Se content is observed, while Ge and Sb concentrations presented a variation of 23.8% and 28.6%, respectively. However, for Se II an increase of the emission intensity with Sb_2Se_3 content was observed. The increased velocities found for Sb rich targets can lead to a higher ionization efficiency of all plasma components through collision processes thus an increase in ionic species. While for Sb II this augmentation is overlaid with the concentration increase, for Ge the composition variation surmounts the enhanced ionization efficiency.

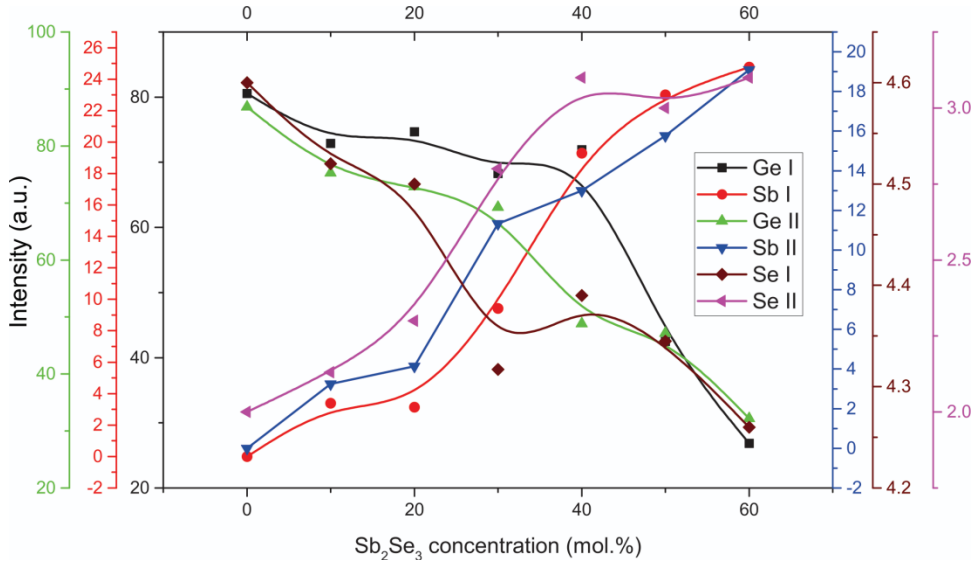

FIG. 5. The evolution of the maximum intensity of the spectral lines of germanium (Ge I, Ge II), antimony (Sb I, Sb II) and selenium (Se I, Se II) with Sb_2Se_3 content at 6 mm distance from the target (25 ns gate delay, 2μs gate width)

In order to obtain information on the excitation mechanism and to study the plasma heterogeneity, the temporal dynamics of the population of excited states of both atoms and ions were analyzed. The spatial and temporal evolution of the emission spectrum lines recorded at different distances in respect to target surface have been analyzed using the fast response photomultiplier (950 V amplifying voltage). An example of emission intensity temporal profiles obtained for Ge and Sb neutrals and ions at a distance of 1 mm from the $Ge_{19.4}Sb_{16,7}Se_{63.9}$ (x=30%) target is presented in Figure 6(a). As the variation of Se concentration in the target is very limited, we focused our study on the more intense Ge and Sb emission lines.

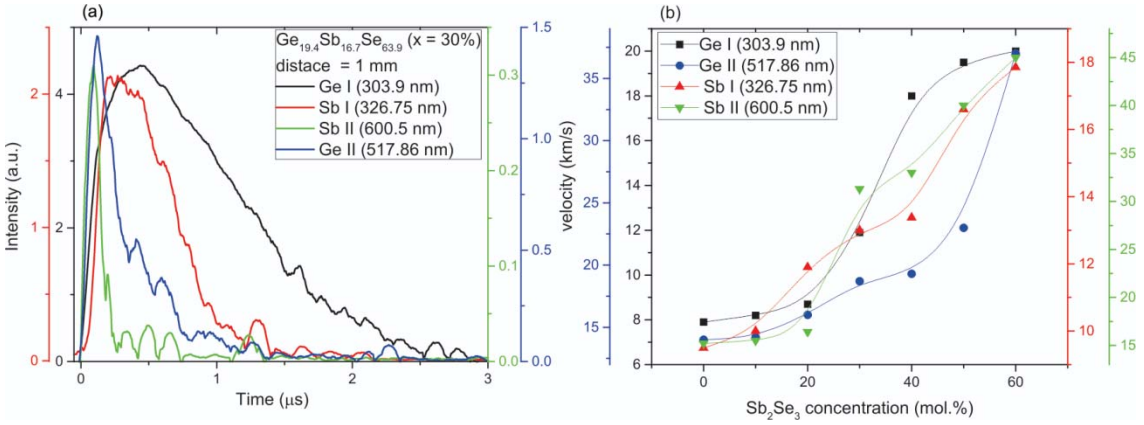

FIG. 6. (a) Temporal evolution of the investigated emission lines at 1 mm from the target and (b) the evolution of the corresponding expansion velocities with the Sb_2Se_3 content

We observe that both Ge and Sb neutrals exhibit a longer emission time than the corresponding ions. The shift of the maximum emission time for each species at different distances allowed us to determine their expansion velocities and their evolution with the Sb_2Se_3 concentration (Figure 6 (b)). The results reveal the presence of energetic ions in the plume with expansion velocities of tens of km/s and neutral species presenting two times lower velocity values. Correlating these results with the ones obtained by ICCD imaging we conclude that while the first structure ("fast" component) consists mainly in ionic species, the second one ("slow" component) is formed predominantly by neutrals with velocities below 20 km/s. As observed for ICCD imaging results, the velocities for Ge and Sb atoms and ions also increased with Sb_2Se_3 content in the bulk sample.

For information on the internal energies of the species present in the plume, the average excitation temperatures were derived from the optical emission spectra using the Boltzmann equation [32]:

$$\ln\left(\frac{\lambda I_{ki}}{A_{ki} g_k}\right) = \left[\frac{4\pi}{N_0 hc} \ln Z(T)\right] - \frac{E_k}{KT},$$

where N_0 is the total number density of atoms in the ground state, g_k the statistical weight of the upper level, E_k is the energy of the upper level and $Z(T)$ is the partition function. An example of the obtained Boltzmann plots for Ge and Sb atoms is given in Figure 7 (a). For a Boltzmann plot of Se, not enough spectral lines with a complete description of the energy level characteristics in the available databases were identified.

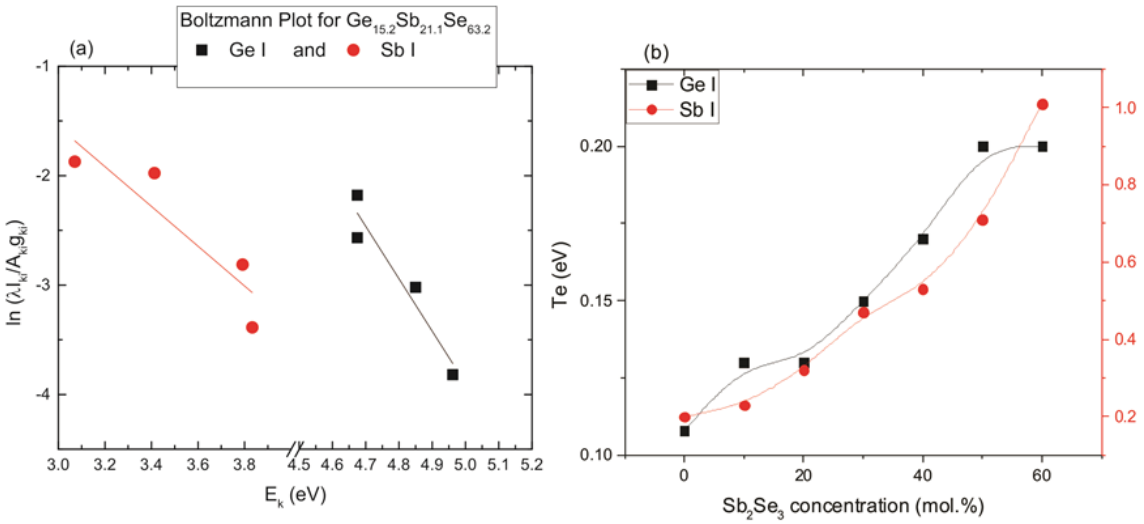

FIG. 7. (a) Boltzmann Plot for the emission lines corresponding to Ge I and Sb I and (b) the excitation temperature dependence on the Sb_2Se_3 concentration at 6 mm from the target surface

Figure 7 (b) presents the evolution of the average excitation temperature for Ge and Sb atoms with the increase of Sb_2Se_3 concentration. The excitation plasma temperature presented a quasi-linear increase with the Sb_2Se_3 content, varying from 0.1eV to 0.2eV for Ge species and from 0.2 eV to 1 eV for Sb species. The differences in excitation temperatures of Ge I and Sb I raise the question of the presence of a local thermodynamic equilibrium in our plasma. Ge and Sb species appear not to be equilibrated in temperature by the (insufficient) collisions subsequent to the initial ejection from the target with different amounts of energy. They seem however thermalized (in Boltzmann sense) individually, at least on the (limited) energy ranges considered (3 – 3.8 eV for Sb and 4.6 – 5 eV for Ge).

4. DISCUSSION

Based on the ICCD imaging and space- and time-resolved optical emission spectroscopy results, the first fast plasma structure is considered to be mainly formed by ionic species while the second one is represented by neutrals. This splitting of the plasma plume was observed for other types of materials [25, 33] and the formation and expansion of each structure is based on distinct ejection mechanisms. The first structure is due to electrostatic interactions as, at very short time scale, the positive charge left on the target surface by electron laser excitation and detachment would accelerate the positive ions outwards the surface. The neutrals found in the second plasma structure are generated through thermal processes that require more time to establish. The low velocity values (<10 km/s) of the third plasma structure is consistent with the presence of nanoparticles, clusters or molecules which have a greater mass and thus a lower mobility compared to the species from the first two plume components.

The main result of this study is the observation of important changes in expansion velocity as well as in emission lines intensity and excitation temperature with the addition of Sb_2Se_3. We propose hereafter an interpretation of these observations based on the structural and electrical/thermal changes in the target. As observed in our previous study on Ge-Sb-Se based bulk chalcogenides [19], the band gap energy presented a decrease from 2.16 to 1.62 eV and the glass transition temperature monotonically decreased with the increase of the Sb_2Se_3 content from 10 to 60 %. The study of Afifi et al. [34] revealed an increase in electrical and thermal conductivity coefficients, together with a decrease in activation energy on the increase in Sb concentration in $Se_{75}Ge_{25-x}Sb_x$ glasses. These compositional evolutions were correlated with the increase of "weak" bond density in the studied system. Considering that the covalent bonds govern the electrical properties, their density decrease leads to a higher conductivity of the Sb rich compounds [34, 35]. This is in agreement with our results reported in [19] on bulk $(GeSe_2)_{100-x}(Sb_2Se_3)_x$ samples where, as x increases, Raman spectroscopy measurements revealed a decrease in peak intensity of Ge-Ge bond vibrations (170 and 270 cm^{-1}) and an increase of 190 cm^{-1} peak contribution corresponding to Sb-Se bond vibration in $[SbSe_{3/2}]$ pyramids.

Since the first plasma structure is mainly formed by electrostatic interactions, the compositional evolution of conductivity can account for the increase of the velocity of the fast plume component with antimony concentration. As the conductivity of the samples increases, a higher concentration of electrons will be ejected through electrostatic mechanisms leading to the formation of an intense positive charge region on the target

surface in the very first moments of the ablation inception. The charge separation leads to a strong ambipolar electric field in which the ions are accelerated. For the second and third plasma structures (containing mostly Ge, Sb and Se neutral atoms), which are formed by thermal processes, the velocity variation can be explained by the decrease in glass transition temperature (thus rigidity of the network [36]) and increase in "weak" bonds density with increasing Sb_2Se_3 content. Thus less energy is needed to melt and vaporize the material and consequently more particles with higher internal and kinetic energy are ejected from the target using the same intensity of the incident radiation. This energy transfer leads to an increase in particle velocity and subsequently in collision and excitation processes which can account for the higher excitation temperatures of Ge and Sb obtained by Boltzmann plot.

5. CONCLUSIONS

ICCD imaging and time- and space-resolved optical emission spectroscopy were used to study the influence of Sb_2Se_3 content on the formation and expansion of plasma formed from $(GeSe_2)_{100-x}(Sb_2Se_3)_x$ chalcogenide glasses, together with the compositional dependence of the excitation temperature. For all glass targets, ICCD images recorded at different delays revealed the presence of three structures with distinct dynamics, which increased their velocities as the Sb_2Se_3 content was augmented. Further results obtained from time-of-flight profiles of the species present in the plume revealed the nature of each plasma structure: the first (fast) plasma structure consists mainly in ionic species with velocity values of tens of km/s, ejected through electrostatic interactions, the second structure, represented by neutral species, with velocity values below 20 km/s, is due to thermal mechanisms and the third structure presenting much lower velocities is formed by nanoparticles and clusters formed by collisions between the backscattered and ejected particles.

The plume characteristics were correlated to the structural and electrical/thermal changes induced by the addition of Sb_2Se_3 in the bulk material. The increased conductivity of antimony-rich samples was associated to the first plasma plume dynamics. The acceleration of the ions found in this plasma structure is considered to be a result of the more intense ambipolar electrical field induced by larger positive region formed by electron ejection. The velocities of the second and third plasma structures and also the excitation temperatures obtained by Boltzmann plots increased as Sb_2Se_3 was added. This behavior was explained by the decrease of the glass transition temperature (network rigidity) of Sb rich samples. As less of the incident energy is used to melt and vaporize the glass, more of it is transferred to

kinetic and internal energy of the ejected particles. The higher kinetic energy is confirmed by the increase in velocity while the higher internal energy is correlated with the increase of the plume species excitation temperatures.

Acknowledgements

Financial support from the Czech Science Foundation (Project No. 15-02634S), the PHC projects Brancusi No. 29551XB and Barrande No. 28449NK, and the POSCCE-O2.2.1, Project No. 257/28.09.2010 (CERNESIM) is greatly acknowledged.

References

[1] B. J. Eggleton, B. Luther-Davies, K. Richardson, Chalcogenide photonics, Nat. Photonics 5 (2011) 141–148;

[2] A. Zakery, S. Elliott, Optical properties and applications of chalcogenide glasses: a review, J. Non-Cryst. Solids 330 (2003) 1–12;

[3] J. -L. Adam, X. Zhang, Chalcogenide Glasses Preparation, Properties and Applications, Woodhead Publishing, 2013;

[4] G. Pfeiffer, M. A. Paesler, S. C. Agarwal, Reversible photodarkening of amorphous arsenic chalcogens, J. Non-Cryst. Solids 130 (1991) 111–143;

[5] K. E. Youden, T. Grevatt, R.W. Eason, H.N. Rutt, R.S. Deol, G. Wylangowski, Pulsed laser deposition of Ga-La-S chalcogenide glass thin film optical waveguides, Appl. Phys. Lett. 63 (1993) 1601;

[6] V. K. Tikhomirov, S. R. Elliott, The anisotropic photorefractive effect in bulk As_2S_3 glass induced by polarized subgap laser light, J. Phys. Condens. Matter. 7 (1995) 1737–1747;

[7] M. Mitkova, M. Kozicki, H. Kim, T. Alford, Thermal and photodiffusion of Ag in S-rich Ge–S amorphous films, Thin Solid Films. 449 (2004) 248–253;

[8] L. Calvez, Z. Yang, P. Lucas, Light-induced matrix softening of Ge-As-Se network glasses, Phys. Rev. Lett. 101 (2008) 177402;

[9] A. V. Kolobov, J. Tominaga, Chalcogenide glasses as prospective materials for optical memories and optical data storage, J. Mater. Sci. Mater. El. 14 (2003) 677–680;

[10] A. Ganjoo, K. Shimakawa, K. Kitano, E. Davis, Transient photodarkening in amorphous chalcogenides, J. Non-Cryst. Solids 299-302 (2002) 917–923;

[11] A. J. Apling, A. J. Leadbetter, A. C. Wright, A comparison of the structures of vapour-deposited and bulk arsenic sulphide glasses, J. Non-Cryst. Solids 23 (1977) 369–384;

[12] H. Nasu, K. Kubodera, M. Kobayashi, M. Nakamura, K. Kamiya, Third-Harmonic Generation from Some Chalcogenide Glasses, J. Am. Ceram. Soc. 73 (1990) 1794–1796;

[13] J. M. Harbold, F. Ö. Ilday, F. W. Wise, B. G. Aitken, Highly nonlinear Ge-As-Se and Ge-As-S-Se glasses for all-optical switching, IEEE Photonic Tech. L. 14 (2002) 822–824;

[14] J. M. Harbold, F. Ö. Ilday, F. W. Wise, J. S. Sanghera, V. Q. Nguyen, L. B. Shaw, I. D. Aggarwal, Highly nonlinear As-S-Se glasses for all-optical switching, Opt. Lett. 27 (2002) 119 – 121;

[15] T. Cardinal, K. Richardson, H. Shim, A. Schulte, R. Beatty, K. Le Foulgoc, C. Meneghini, J. F Viens, A. Villeneuve, Non-linear optical properties of chalcogenide glasses in the system As–S–Se, J. Non-Cryst. Solids. 256-257 (1999) 353–360;

[16] G. Lenz, S. Spalter, Chalcogenide Glasses, in R. E. Slusher, B. J. Eggleton (Eds.) Nonlinear Photonic Crystals, Springer Series in Photonics, 2003, pp. 255–267.
[17] Y. Chen, X. Shen, R. Wang, G. Wang, S. Dai, T. Xu, Q. Nie, Optical and structural properties of Ge-Sb-Se thin films fabricated by sputtering and thermal evaporation, J. Alloy. Compd. 548 (2013) 7–12;
[18] G. Boudebs, S. Cherukulappurath, M. Guignard, J. Troles, F. Smektala, F. Sanchez, Experimental observation of higher order nonlinear absorption in tellurium based chalcogenide glasses, Opt. Commun. 232 (2004) 417–423;
[19] M. Olivier, J. C. Tchahame, P. Němec, M. Chauvet, V. Besse, C. Cassagne, G. Boudebs, G. Renversez, R. Boidin, E. Baudet, V. Nazabal, Structure, nonlinear properties, and photosensitivity of $(GeSe_2)_{100-x}(Sb_2Se_3)_x$ glasses, Opt. Mater. Express. 4 (2014) 525;
[20] V. Nazabal, F. Charpentier, J. -L. Adam, P. Nemec, H. Lhermite, M. -L. Brandily-Anne, J. Charrier, J. -P. Guin, A. Moréac, Sputtering and Pulsed Laser Deposition for Near- and Mid-Infrared Applications: A Comparative Study of $Ge_{25}Sb_{10}S_{65}$ and $Ge_{25}Sb_{10}Se_{65}$ Amorphous Thin Films, Int. J. Appl. Ceram. Tec. 8 (2011) 990–1000;
[21] F. Verger, V. Nazabal, F. Colas, P. Němec, C. Cardinaud, E. Baudet, R. Chahal, E. Rinnert, K. Boukerma, I. Peron, S. Deputier, M. Guilloux-Viry, J. P. Guin, H. Lhermite, A. Moreac, C. Compère, B. Bureau, RF sputtered amorphous chalcogenide thin films for surface enhanced infrared absorption spectroscopy, Opt. Mater. Express. 3 (2013) 2112;
[22] M. Frumar, B. Frumarova, P. Nemec, T. Wagner, J. Jedelsky, M. Hrdlicka, Thin chalcogenide films prepared by pulsed laser deposition - new amorphous materials applicable in optoelectronics and chemical sensors, J. Non-Cryst. Solids 352 (2006) 544–561;
[23] J. Schou, Physical aspects of the pulsed laser deposition technique: The stoichiometric transfer of material from target to film, Appl. Surf. Sci. 255 (2009) 5191–5198;
[24] O. G. Pompilian, G. Dascalu, I. Mihaila, S. Gurlui, M. Olivier, P. Nemec, V. Nazabal, N. Cimpoesu, C. Focsa, Pulsed laser deposition of rare-earth-doped gallium lanthanum sulphide chalcogenide glass thin films, Appl. Phys. A 117 (2014) 197–205;
[25] O. G. Pompilian, S. Gurlui, P. Nemec, V. Nazabal, M. Ziskind, C. Focsa, Plasma diagnostics in pulsed laser deposition of GaLaS chalcogenides, Appl. Surf. Sci. 278 (2013) 352–356;
[26] M. Olivier, P. Němec, G. Boudebs, R. Boidin, C. Focsa, V. Nazabal, Photosensitivity of pulsed laser deposited Ge-Sb-Se thin films, Opt. Mater. Express. 5 (2015) 781;
[27] C. Focsa, P. Nemec, M. Ziskind, C. Ursu, S. Gurlui, V. Nazabal, Laser ablation of As_xSe_{100-x} chalcogenide glasses: Plume investigations, Appl. Surf. Sci. 255 (2009) 5307–

5311;
[28] S. Canulescu, E. L. Papadopoulou, D. Anglos, T. Lippert, C. W. Schneider, A. Wokaun, Mechanisms of the laser plume expansion during the ablation of $LiMn_2O_4$, J. Appl. Phys. 105 (2009) 063107;
[29] S. Amoruso, R. Bruzzese, N. Spinelli, R. Velotta, M. Vitiello, X. Wang, G. Ausanio, V. Iannotti, L. Lanotte, Generation of silicon nanoparticles via femtosecond laser ablation in vacuum, Appl. Phys. Lett. 84 (2004) 4502;
[30] NIST Atomic Spectra Database, http://physics.nist.gov;
[31] S. Gurlui, O. Niculescu, D. G. Dimitriu, C. Ionita, R. W. Schrittwieser, Elementary processes in the dynamics of two simultaneously excited fireballs in plasma, Int. J. Mass Spectrom. 365-366 (2014) 42-47;
[32] W.-H. Wei, L. Fang, X. Shen, R.-P. Wang, Crystallization kinetics and thermal stability in Ge-Sb-Se glasses, Phys. Status Solidi B 250 (2013) 59–64;
[33] C. Ursu, O. G. Pompilian, S. Gurlui, P. Nica, M. Agop, M. Dudeck, C. Focsa, Al_2O_3 ceramics under high-fluence irradiation: plasma plume dynamics through space- and time-resolved optical emission spectroscopy, Appl. Phys. A 101 (2010) 153–159;
[34] M. A. Afifi, H. H. Labib, M. H. El-Fazary, M. Fadel, Electrical and Thermal Properties of Chalcogenide Glass System $Se_{75}Ge_{25-x}Sb_x$, Appl. Phys. A 55 (1992) 167–169;
[35] A. Giridhar, P. S. L. Narasimham, S. Mahadevan, Density and microhardness of Ge-Sb-Se glasses, J. Non-Cryst. Solids 43 (1981) 29–35;
[36] R. J. Freitas, K. Shimakawa, S. Kugler, Some remarks on the glass-transition temperature in chalcogenide classes : a correlation with the microhardness, Chalcogenide Lett. 10 (2013) 39–43.